Case Studies in Construction Materials 22 (2025) e04426

Contents lists available at ScienceDirect

Case Studies in Construction Materials

journal homepage: www.elsevier.com/locate/cscm

The effect of adding rice husk ash (RHA) and calcined shell powder (CSP) on the properties of cement mortar

J.X. Zhang [a], Y.T. Guo [a,*], S.Y. Zhuang [b], H.Q. Lou [c], Y. Li [c]

[a] Shenzhen International Graduate School, Tsinghua University, Shenzhen, China
[b] Department of Civil and Environmental Engineering, The Hong Kong Polytechnic University, Kowloon, Hong Kong, China
[c] School of Civil and Environmental Engineering, Harbin Institute of Technology, Shenzhen, China

ARTICLE INFO

Keywords:
Rice husk ash
Calcined shell powder
Pozzolanic reaction
C-S-H
Composite cement

ABSTRACT

To enhance sustainability in the construction industry, incorporating rice husk ash (RHA) as a partial cement replacement is widely encouraged. Additionally, bio-shells, rich in $CaCO_3$, pose environmental challenges when improperly discarded, leading to pollution and negative impacts on surrounding communities. This study integrates the beneficial properties of these two waste materials for use in construction. While the effects of RHA on cementitious materials have been extensively studied, limited research has examined the combined influence of RHA and calcined shell powder (CSP) as a partial cement replacement. To explore their potential, RHA and CSP were blended in varying proportions to produce RHA-CSP cement mortar. Experimental results demonstrated that the R15S10 mix achieved the highest mechanical performance by optimizing the balance between pozzolanic reactivity and the filler effect. As hydration progressed, the pozzolanic reaction intensified under high pH conditions, increasing the C-S-H dehydration peak while reducing the CH decomposition peak. Additionally, the incorporation of CSP and RHA refined the pore structure and decreased overall porosity, enhancing mortar compactness. By utilizing these waste materials to create an optimized mix, this study supports the sustainable application of discarded shells and rice husks in construction.

1. Introduction

Compared to timber, masonry, and steel materials, concrete offers several advantages, including ease of shaping, low cost, abundant raw materials, and wide applicability [1,2]. As a result, it has become one of the most widely used materials in civil engineering [3–5]. However, cement, a key component in concrete, requires extensive natural resources and energy for production while also emitting significant amounts of CO_2 and other pollutants, contributing to environmental degradation and posing risks to human health [8]. Addressing these environmental concerns has led to a growing emphasis on sustainability in concrete research and industry [9].

One approach to improving sustainability is the incorporation of waste materials from various sources, including agriculture and aquaculture, as partial replacements for conventional concrete constituents [5–7,10,11]. Studies have demonstrated that utilizing industrial and agricultural by-products can enhance concrete durability while reducing its environmental footprint. For instance,

* Corresponding author.
E-mail addresses: zjx1215147501@163.com (J.X. Zhang), guoyutao@sz.tsinghua.edu.cn (Y.T. Guo), mini_zhuang@163.com (S.Y. Zhuang), Louhqhitsz@163.com (H.Q. Lou), liye@hit.edu.cn (Y. Li).

https://doi.org/10.1016/j.cscm.2025.e04426
Received 24 October 2024; Received in revised form 11 February 2025; Accepted 18 February 2025
Available online 20 February 2025

research on basalt fiber-reinforced concrete highlights its potential to improve long-term durability and mechanical performance in sustainable construction [12]. Similarly, life cycle assessments of alternative cementitious materials, such as fly ash and silica fume, reveal significant reductions in global warming potential and carbon emissions [13]. Even utilization of green or recycled components in concrete might reduce the strengths, combining it with stiffening layers in composite constructions offering flexible applications [14–16]. Among agricultural by-products, rice husks are rich in active silica and are widely available. However, their disposal remains a challenge, as high transportation costs and low nutrient content limit their reuse, leading to widespread open-field burning, which contributes to air pollution [17,18]. Similarly, China, the world's largest shellfish producer, generates approximately 10 million tons of discarded shells annually, most of which are landfilled, causing environmental pollution and negatively affecting local communities [19]. Bio-shells are abundant in $CaCO_3$, posing environmental pollution problems and negatively impacting residents' quality of life when they are discarded and accumulated haphazardly [20,21]. Additionally, advancements in predictive modeling techniques, such as machine learning-based symbolic regression and GRG-optimized response surface methods, have enabled the optimization of mix designs for enhanced performance and sustainability [22–24]. These approaches provide valuable tools for assessing the mechanical and microstructural properties of novel cementitious composites, including those incorporating RHA and CSP.

The integration of rice husk ash (RHA) and calcined shell powder (CSP) in cementitious materials has the potential to reduce the consumption of traditional raw materials while simultaneously mitigating waste disposal issues. Although previous studies have investigated the effects of individual waste materials on concrete properties, limited research has explored the combined impact of RHA and CSP in cement mortar. Therefore, this pioneer study aims to address this gap by examining the effects of RHA and CSP on the properties of cement mortar, offering new insights into the sustainable development of construction materials.

RHA is the solid residue left after burning rice husks, mainly composed of silica [17,25,26]. RHA plays an important role in workability and fluidity during early curing because its irregular and porous particle morphology enhances water retention and reduces paste lubricity [25]. In the hardened state, RHA grains act as micro-fillers, increasing the compactness and reducing the porosity of concrete. During medium and long-term hydration, RHA serves as a raw material for the pozzolanic reaction, producing C-S-H gel that enhances compressive strength. Due to its small particle size, RHA also provides more nucleation sites for the hydration products, accelerating the hydration of cement clinker [27,28]. To obtain RHA with high-activity silica, the combustion temperature of rice husks must be strictly controlled. Studies have shown that RHA has the highest pozzolanic activity when the combustion temperature is between 500°C and 800°C [29]. The cementitious reaction of RHA also depends on its particle size, with finer RHA exhibiting stronger reactivity [4,30]. On the other side, among the total shell waste in China, more than 300,000 tons of oyster shells are discarded annually, but only 30 % are reused [31,32]. Due to the high $CaCO_3$ content in shells, they decompose into CaO under high-temperature calcination, enabling them to substitute part of the cementitious material while also reducing the carbon content within the matrix [33]. At high temperatures, $CaCO_3$ transforms into CaO, which reacts rapidly with water to form calcium hydroxide (CH) in cement-based mixtures [34]. If the mixtures contain silica, a pozzolanic reaction can occur between the two, forming C-S-H gel that increases strength, fills voids, and enhances durability [3,35].

During the cement hydration process, RHA consumes free CH and forms C-S-H gel due to its high fineness and reactivity. The unsaturated surface of RHA grains provides nucleation sites for cement hydration and the formation of hydration products, which accelerates the hydration reaction in RHA-cement composites [36–38]. Theoretically, the more RHA added, the more pozzolanic reaction products will be produced. However, if the substitution level of RHA is increased to the point where the alkaline activation effect of the cement is weakened, the reactivity of RHA may decrease [39]. The amount of CH produced by cement hydration depends on the composition of the cement. Replacing part of the cement with CSP can increase the pH value of the matrix, thereby improving the overall performance of the mixtures [20]. Besides, under high levels of RHA substitution, the presence of additional CH reduces the risk of self-neutralization of the matrix. The presence of CH increases the concentration of calcium ions, contributing to the early formation of reaction products. Additionally, the presence of CH increases the concentration of OH- ions, which act to break the chemical bonds of RHA, thereby accelerating the pozzolanic reaction [36]. It has been explained that PH has a significant impact on the pozzolanic activity of RHA, indicating that the spherical structure of RHA only decomposes extensively when the pH exceeds approximately 13.2 or 13.3 [40]. pH can be used to indicate the pozzolanic activity of a substance. A decrease in pH indicates that a pozzolanic reaction has occurred in the matrix. The lower the pH, the higher the degree of pozzolanic reaction [41].

This study combines two types of wastes from agriculture and aquaculture to produce highly active and finely sized RHA and CSP through controlled temperature-time burning, grinding, and sieving. These green materials aim to partially replace cement in construction, thereby reducing the economic and environmental impacts of cement production. Efforts in this study have been made to develop sustainable cementitious materials by incorporating wastes into cement mixes. Although previous studies have investigated the effects of RHA and CSP individually, limited research has explored their combined influence on cement mortar properties. This study specifically examines the synergistic effects of RHA and CSP in optimizing hydration reactions, refining pore structure, and improving mechanical performance. Based on analysis tools of mechanical tests, Thermogravimetric Analysis (TGA), Mercury Intrusion Porosimetry (MIP), Scanning Electron Microscope (SEM), etc., the key material properties of ultimate strengths, phase composition changes, and microstructure developments were extensively explored. To bridge the research gap, this study evaluates the interactions between RHA and CSP at different replacement levels, identifying how their combination influences cement hydration and mortar densification. The test design aimed to determine the optimal mix ratio of RHA and CSP to maximize cement mortar performance, clarify the underlying mechanisms governing their pozzolanic and filler effects, and understand the role of RHA and CSP when partially replacing cement. By providing comprehensive insights into their combined application, this study contributes to the advancement of alternative cementitious materials. It will promote the use of discarded shells and rice husks in the construction industry.

2. Experimental program

2.1. Materials

This study utilized cement, RHA, and CSP as the cementitious materials, with ISO standard sand employed as the fine aggregates. To ensure excellent workability, an appropriate quantity of polycarboxylate superplasticizer (SP) was added. The cement was a 42.5 R high early strength type from Yan Hong Trading Co., Ltd. The raw rice husks were provided by Tianfu Granary in Dongpo District, Meishan City, Sichuan Province, and the oyster shells were supplied by an oyster farming base in Zhanjiang City, Guangdong Province. ISO standard sand was produced and supplied by Xiamen ISO Co., Ltd. The polycarboxylate superplasticizer, provided by Muhu Co., Ltd., had a solid content of 24 % and achieved a water reduction rate of approximately 25 %. Tap water from the laboratory was used for all the mixtures. The chemical compositions of the cement, CSP, and RHA, determined by X-ray fluorescence analysis, are detailed in Table 1. Fig. 1 presents the particle size distribution curves of the various powders and aggregates utilized during the specimen preparation. RHA has an average particle size of 5.12μm and an amorphous phase content of 70.7 %. CSP is composed of 97.339 % CaO, with an average particle size of 8.54μm.

To ensure the high reactivity of RHA and CSP, precise control of burning temperature and duration is essential [3]. While uncontrolled combustion is cost-effective and easy to replicate, improper burning can result in RHA with excessive unburned carbon and crystalline silica, which negatively affects strength [1]. Supplementary cementitious materials with high carbon content and crystallinity are generally considered poor cement replacements. Particle size also plays a crucial role in mortar performance [28]. Larger CSP grains slow down dissolution, thereby reducing the pozzolanic reaction rate. Similarly, coarse RHA particles lead to an uneven distribution of nucleation sites, hindering reactivity [30]. Moreover, larger RHA grains primarily function as pore fillers rather than reactive components, further increasing porosity and decreasing mortar strength and durability [4]. Fig. 2 presents unburned shells and raw rice husks.

The pozzolanic activity of RHA is closely linked to its silica content and crystallinity. Crystalline and semi-crystalline silica significantly impact the reaction with CH [1]. Fig. 3 displays XRD images of CSP and RHA, showing RHA's high amorphous content and CSP's high CaO content. Studies indicate that incinerating RHA and CSP between 500°C and 800°C yields amorphous silica, while temperatures above 800°C lead to crystallization, reducing pozzolanic efficiency [8]. This phase transformation results in cristobalite or tridymite, lowering reactivity [5].

For material preparation, purified rice husks, free from impurities, were heated in a muffle furnace. The temperature was gradually raised at 5°C /min to 500°C, held for one hour, then increased to 800°C, where it was maintained for three hours before natural cooling [42]. Similarly, cleaned and dried oyster shells were heated at 10°C /min to 1000°C and maintained for three hours before cooling [43]. After burning, RHA was sieved through a 300-mesh sieve, while CSP was sieved through a 325-mesh sieve. Fig. 4 illustrates RHA after combustion and CSP after grinding and sieving.

2.2. Mix design

The mix proportions with different amounts of RHA and CSP are shown in Table 2. The water-to-binder ratio is 0.3 [44,45], maintaining the mass ratio of the raw materials as cementitious materials: standard sand: water = 1: 1.6: 0.3. Ten different mix proportions with varying replacement levels of RHA and CSP were studied. RHA replaced cement at mass ratios of 0 %, 10 %, 15 %, and 20 %, while CSP replaced cement at mass ratios of 0 %, 5 %, 10 %, and 15 %. The amount of SP varied in each mix proportion to ensure the slump remained approximately 240 mm.

2.3. Specimens preparation and curing

The specimen materials were prepared using a 20 L mortar mixer to ensure uniformity and consistency. Before mixing, the mixer walls and blades were wiped with a damp cloth to create a pre-wetted surface, preventing excessive water absorption during mixing.

Table 1
Chemical properties of cementitious materials.

Oxides (%)	OPC	RHA	CSP
Na_2O	0.28	0.04	0.73
MgO	6.06	0.55	0.75
Al_2O_3	10.67	0.37	0.08
SiO_2	24.23	93.15	0.17
P_2O_5	0.13	0.88	0.13
SO_3	4.66	0.61	0.44
Cl	0.01	0.09	0.09
K_2O	0.93	3.45	0.02
CaO	49.25	0.67	97.34
TiO_2	0.91	–	–
MnO	0.11	0.12	–
Fe_2O_3	2.61	0.04	0.07
ZnO	–	0.01	0.02

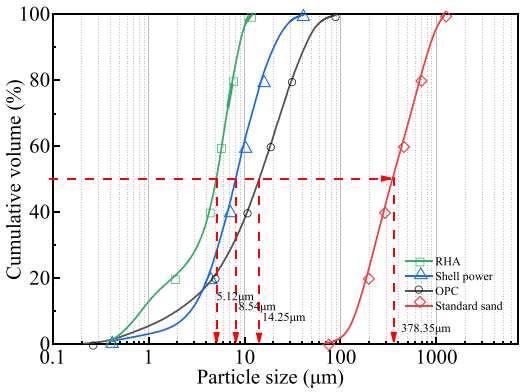

Fig. 1. Particle size distribution of the materials.

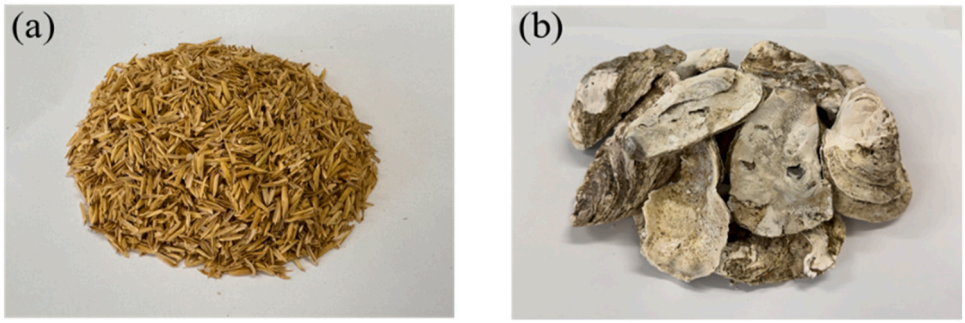

Fig. 2. Raw rice husks (a) and shells (b).

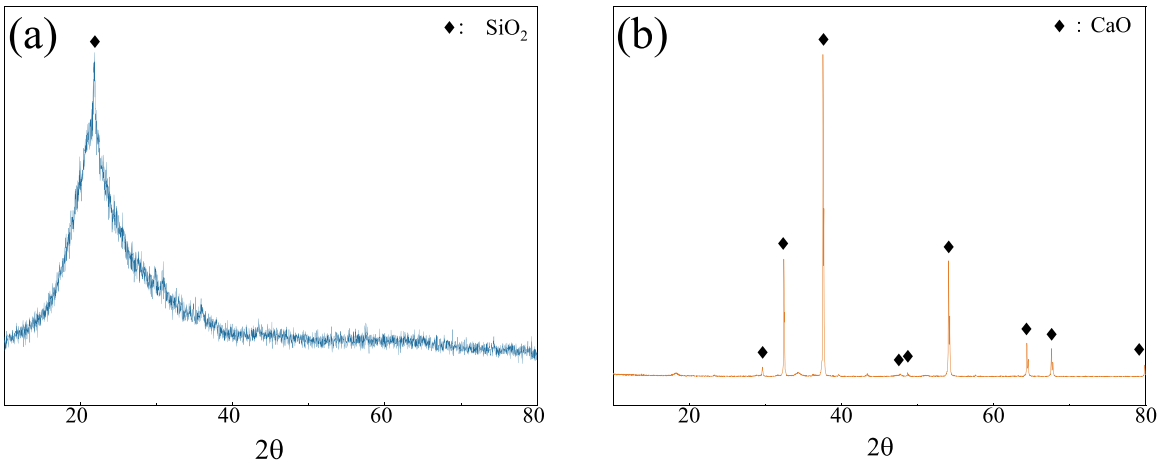

Fig. 3. XRD of RHA (a) and CSP (b).

CSP was first mixed with water and left to stand for 30 min to allow the exothermic reaction to complete. Cement, RHA, and standard sand were then sequentially introduced, with fine aggregates placed on top of the cementitious materials to minimize material loss during the initial mixing phase. The dry components were mixed at low speed for 3 min to ensure even dispersion of cementitious materials and aggregates [46,47]. Subsequently, the fully reacted CSP-water mixture and SP were gradually incorporated and mixed at high speed for an additional 3 min to achieve a homogenous mortar. The freshly mixed cement mortar was then poured into $40 \times 40 \times 160$ mm^3 prism triplet molds. After initial setting, the specimens were covered with plastic film and allowed to stand for 24 h before demolding. Finally, the specimens were cured in water at 20 ± 3°C, with subsequent tests conducted at 7 and 28 days to evaluate performance.

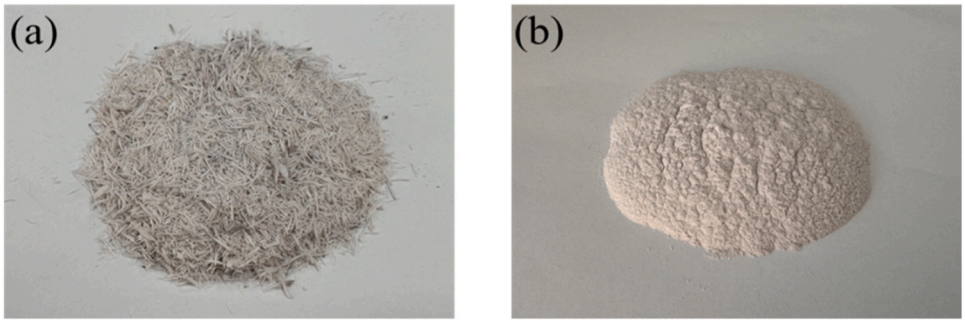

Fig. 4. RHA after burning (a) and CSP after grinding and sieving (b).

Table 2
Mixture design.

Mixture design	Replacement		Cement	Sand	SP
	RHA (%)	CSP (%)			
R0S0	0 %	0 %	100 %	100 %	0.32 %
R10S5	10 %	5 %	85 %	100 %	0.34 %
R10S10	10 %	10 %	80 %	100 %	0.36 %
R10S15	10 %	15 %	75 %	100 %	0.38 %
R15S5	15 %	5 %	80 %	100 %	0.36 %
R15S10	15 %	10 %	75 %	100 %	0.38 %
R15S15	15 %	15 %	70 %	100 %	0.40 %
R20S5	20 %	5 %	75 %	100 %	0.38 %
R20S10	20 %	10 %	70 %	100 %	0.40 %
R20S15	20 %	15 %	65 %	100 %	0.42 %

2.4. Testing

2.4.1. Compressive strength test

The compressive strength tests in this study were carried out in accordance with GB/T 17671–2021 [48]. After reaching the designated curing age, four specimens were placed in a 600 KN universal testing machine and subjected to a constant loading rate of 2.4 KN/s until failure. The maximum load was then recorded.

2.4.2. Scanning electron microscope

A Phenom Prox G6 scanning electron microscope (SEM) was used to analyze microstructural variations in specimens with different mix proportions. Backscattered electron (BSE) mode was employed for imaging.

2.4.3. Mercury intrusion porosimetry

Mercury intrusion porosimetry (MIP) was performed using a Micromeritics Autopore IV 9500 to analyze porosity and pore size distribution in mortar samples. Specimens were taken from the center, subjected to ultrasonic cleaning, and immersed in isopropanol for 24 h to halt hydration. After drying in a vacuum oven at 40°C, MIP tests generated cumulative porosity curves and differential pore size distribution curves to evaluate changes in total porosity and pore structure across different mix proportions and curing ages.

2.4.4. Thermogravimetric analysis

Thermogravimetric analysis (TGA) was conducted using a PerkinElmer STA 8000 to assess mass loss linked to the decomposition of chemical components during heating, providing insights into phase changes and hydration product formation over curing ages. Samples were collected from a 10 mm depth, ultrasonically cleaned, and immersed in isopropanol for 24 h to halt hydration. After drying in a vacuum oven at 40°C, they were ground, sieved through a 200-mesh sieve, and heated at 10°C /min up to 1000°C in a nitrogen atmosphere to prevent carbonization.

3. Results

3.1. Fresh state properties

The final column of Table 2 lists the required SP dosage for each mixture to achieve the target slump, as shown in Fig. 5. Fig. 6 presents SEM images of RHA and CSP, revealing their porous, honeycomb-like structures, which indicate high specific surface area and porosity. The study found that higher RHA replacement levels increased SP demand to maintain the desired workability of 240 mm

± 5 %. During cement hydration, water absorbed in the pore structure promotes Ca^{2+} accumulation on RHA surfaces, leading to CH formation. The amorphous silica in RHA reacts with CH to generate additional C-S-H gel [25]. RHA influences cement hydration through dilution, chemical, and internal curing effects. Dilution occurs due to reduced cement content, while the pozzolanic reaction between silica and CH enhances cementitious properties. Additionally, RHA gradually releases water, promoting continuous hydration [8,26]. As RHA content increases, these effects collectively contribute to a higher SP demand to maintain optimal workability.

As observed in Fig. 5, the higher CSP content, the more SP is required. The reason is that CSP primarily consists of CaO, which reacts intensely with free water to produce CH. During the mortar mixing process, the fine CH grains occupy the voids between the cement grains, restricting water flow and increasing the water retention of the fresh cement mortar. This indirectly acts as a dispersing agent, preventing mortar flocculation and increasing the plasticity of the mixture [36]. Adding RHA and CSP into the mortar can reduce workability because they absorb some of the mixing water due to their high reactivity, attracting water molecules to the substance grains. Extra SP is required to adjust for the reduced free water to achieve the desired workability [37,38].

3.2. Compressive strength

Table 3 presents the compressive strength of 10 different mixtures with varying RHA and CSP contents at 7 and 28 days of curing. At 7 days, all modified mixtures exhibited lower compressive strength than the control, primarily due to the slow pozzolanic reaction and reduced cement content [49]. By 28 days, compressive strength increased across all mixtures, with most RHA-CSP blends surpassing the control. The only exception was R20S15, which, despite achieving 82.21 MPa at 28 days (lower than the control's 84.60 MPa), exhibited a 31.39 % strength increase—substantially higher than the control's 11.81 %.Statistical analysis using one-way ANOVA confirmed significant differences among the mixtures ($p < 0.05$). Post-hoc analysis further revealed that R15S10 exhibited the highest mechanical properties at both curing ages, with a compressive strength of 75.40 MPa at 7 days and 98.60 MPa at 28 days. To further assess the influence of different replacement levels, R15 and S10 were used as benchmarks in a controlled variable analysis (Fig. 7).

Fig. 8 shows the compressive strength and percentage increase of mixtures at different curing ages, considering only the effect of changing the amount of CSP on mortar performance. Adding CSP to mixtures containing 15 % RHA can improve compressive strength, with the optimal performance observed at a 10 % addition. At 7 days, R15S10 exhibited the highest compressive strength, which was still 0.3 MPa lower than the control's. At 28 days, the added CSP participated in the pozzolanic reaction with RHA, generating C-S-H gel, which enhanced the compressive strength of the mixtures. The addition of CSP was observed to be less effective during short curing ages, possibly because the CH produced during cement hydration is sufficient to facilitate the reaction of RHA [50]. Furthermore, high cement content leads to the formation of a substantial amount of cementitious products during the cement hydration process. Consequently, the pozzolanic products generated during short curing ages have a negligible impact on the compressive strength [36,51].

R15S10 and R15S5 showed the highest strength gains, reaching 98.6 MPa (30.77 % increase) and 93.2 MPa (31.27 % increase), significantly exceeding the control's 11.81 %. While R15S15 had a lower 7-day strength due to reduced cement content, its strength gain at 28 days (31.23 %) was still notable [36,52]. Excessive CSP content, however, may lead to CH leaching during curing, negatively impacting strength. As the pozzolanic reaction progresses more slowly than cement hydration, extended curing mitigates CH leaching effects and promotes strength development.

Fig. 9 illustrates the effect of RHA content on the compressive strength of cement mortar at different curing ages. Partial replacement of cement with RHA enhances compressive strength due to its filler effect, which refines the interfacial transition zone. Additionally, the C-S-H gel formed by the pozzolanic reaction improves particle packing and reduces larger pore volumes [53]. At 7 days, the compressive strength of all RHA-containing mixtures was lower than the control, with the most significant reduction being

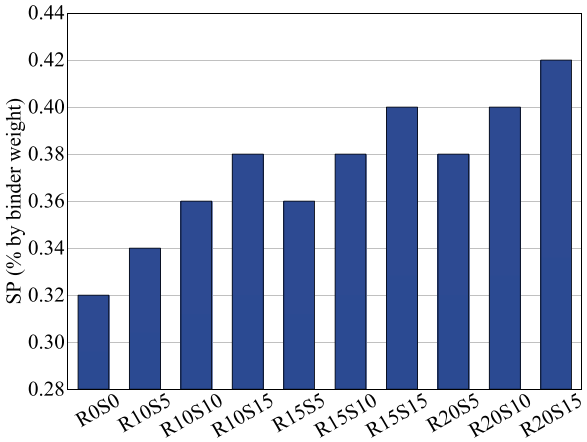

Fig. 5. SP dosage of mixtures to obtain target workability.

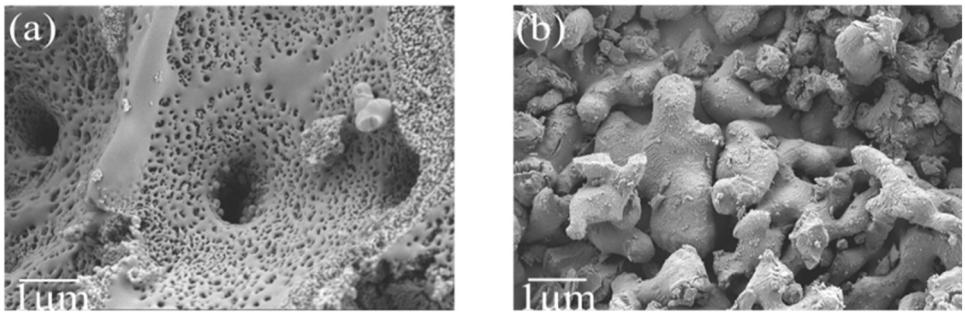

Fig. 6. SEM of RHA (a) and CSP (b).

Table 3
Compressive strength.

Mixture design	Compressive strength (MPa)	
	7d	28d
R0S0	75.67	84.60
R10S5	65.23	88.07
R10S10	69.53	92.77
R10S15	67.78	86.40
R15S5	70.95	93.16
R15S10	75.40	98.60
R15S15	68.16	89.48
R20S5	69.21	91.13
R20S10	72.90	94.22
R20S15	62.57	82.21

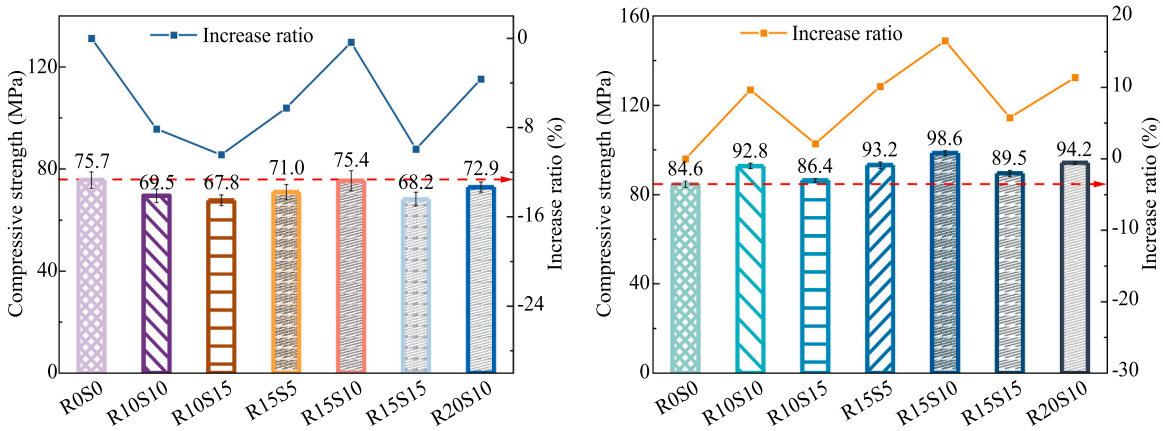

Fig. 7. Compressive strength of seven mixture designs at 7d (a)and28d (b).

6.2 MPa (90.09 % of the control). However, at 28 days, the pozzolanic reaction significantly improved strength, with percentage increases ranging from 29.22 % to 33.53 %. R10S10 exhibited the highest strength gain, increasing from 69.5 MPa to 92.8 MPa, surpassing the control by 9.69 %. R15S10 also demonstrated substantial improvement, with a strength increase from 75.4 MPa to 98.6 MPa (30.77 %). The delayed strength development is attributed to the dormant phase before the pozzolanic reaction initiates, during which boundary reactions and diffusion processes occur, leading to a more pronounced contribution to later-stage strength development [54].

As the RHA content increased from 15 % to 20 %, the 28-day compressive strength of the mortar slightly decreased. The pozzolanic activity and filler effect are critical factors in determining the optimal percentage of cement replacement [55]. The excessive addition of RHA results in a reduced percentage increase in compressive strength. Due to RHA present in the mixture being higher than the CH content in the cement matrix, leading to an accumulation of excess RHA [56]; the increased RHA content results in insufficient cement [57]. Comparatively, R15S10 demonstrates optimal overall mechanical properties. The higher the content of RHA and CSP, the greater the water demand under identical mixing and casting conditions, requiring an increased amount of SP.

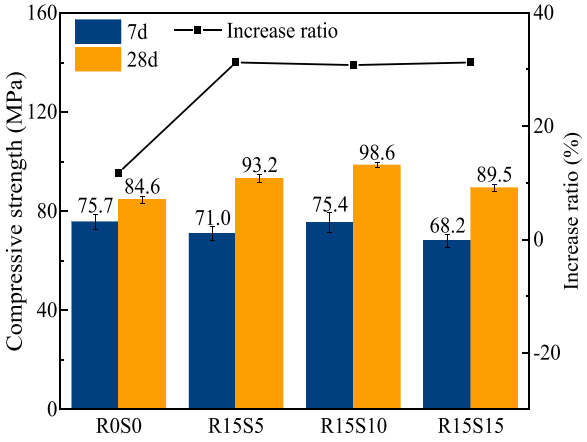

Fig. 8. Compressive Strength Comparison of R0S0, R15S5, R15S10, and R15S15.

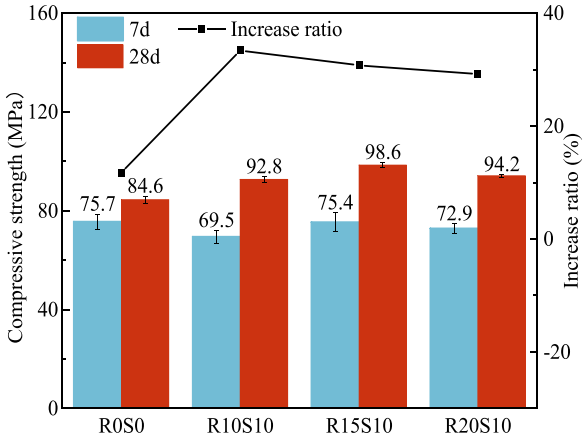

Fig. 9. Compressive Strength Comparison of R0S0, R10S10, R15S10, and R20S10.

3.3. Thermogravimetric analysis

Thermogravimetric analysis (TGA) is a widely used technique for assessing the thermal stability and composition of materials. However, in cement-based materials, its reliability in distinguishing hydration compounds is limited due to overlapping decomposition peaks. The decomposition of cement hydrates appears as mass loss on the TG curve and corresponding endothermic peaks on the DTG

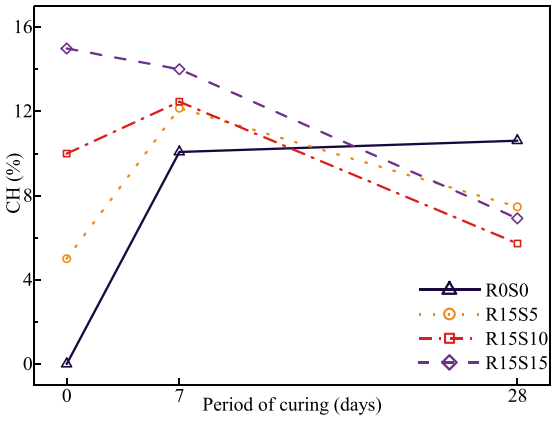

Fig. 10. Free CH (%) of R0S0, R15S5, R15S10, and-0 R15S15.

curve [58]. Fig. 11 and Fig. 13 present the TG and DTG curves of mortar at different curing ages. Cement hydrate decomposition occurs in three stages: 140–400°C (C-S-H and other hydrate dehydration, Ldh), 400–520°C (CH dehydroxylation, Ldx), and 520–1000°C ($CaCO_3$ decarbonation, Ldc). The relative mass loss of cementitious material from $CaCO_3$ decomposition between 600–780°C is denoted as Ldca [59]. Table 4 summarizes the relative mass loss values in each decomposition region from cement paste samples. Hydration alters the solid matrix due to admixture effects, and DTG/TG analyses help elucidate the influence of external admixtures on cement mortar hydration. Following the method of Pane et al. [59], the residual CH content was quantified to determine the extent of the pozzolanic reaction involving CSP.

Fig. 10 presents the residual CH content in the hydration system at different curing ages, highlighting the influence of CSP content on mortar performance. The results indicate that increasing CSP leads to higher CH content at all curing ages. However, with the addition of RHA, CH content decreases over time due to the ongoing pozzolanic reaction. At 7 days, CH content was 12.16 % in R15S5 (7.16 % higher than the initial CSP content), 12.46 % in R15S10 (2.46 % higher), and 14.01 % in R15S15 (0.99 % lower), suggesting that CH from both cement hydration and CSP was consumed by the pozzolanic reaction. The reaction intensity is closely related to pH, as RHA exhibits substantial decomposition only when the pH exceeds approximately 13.2–13.3 [60]. At 28 days, R15S15 exhibited lower compressive strength and a reduced C-S-H dehydration peak compared to R15S5 and R15S10. This is attributed to excessive CSP, leading to surplus CH beyond what is required for the RHA reaction, coupled with a lower cement content. Fig. 11 further reveals that despite R0S0 having a higher C-S-H dehydration peak than R15S5 and R15S15, its compressive strength was the lowest. This highlights the role of C-S-H gel formation and RHA pore filling in enhancing matrix compactness and compressive strength [36].

Fig. 12 and Fig. 13 illustrate the effect of RHA content on CH consumption and pozzolanic activity. At 7 days, R10S10 exhibited the highest CH content (13 %), exceeding the control (10.07 %), while R15S10 and R20S10 had lower CH contents but higher dehydration peaks, indicating early pozzolanic activity. The CH contents of R10S10, R15S10, and R20S10 were 13 %, 12.46 %, and 12.16 %, respectively, exceeding the CSP dosage by 3 %, 2.46 %, and 2.16 %. At 28 days, CH content decreased to 8.31 %, 5.72 %, and 7.24 %, respectively, demonstrating intensified pozzolanic reactions over time. R15S10 exhibited the highest CH consumption, reducing CH by 42.78 % relative to its initial CSP dosage, leading to substantial C-S-H gel formation. This explains its superior compressive strength compared to R10S10 and R20S10, highlighting an optimal balance between pozzolanic activity and filler effects.

At 28 days, the remaining CH in R20S10 was 1.51 % higher than in R15S10. As shown in Fig. 13, the dehydration peak of R20S10 was almost identical to that of R10S10 at 7 days, but its compressive strength was higher than that of R10S10. It could be attributed to the added RHA partially filling the voids and microcracks, which enhances the compressive strength. At 28 days, the dehydration peak of R20S10 was higher than that of R15S10, but its compressive strength was lower than that of R15S10. This is due to the produced C-S-H gel being relatively loose, as well as the low cement content.

3.4. Mercury intrusion porosimetry

The MIP test can obtain cumulative porosity curves and differential pore size distribution curves, allowing for the analysis of changes in total porosity and pore size distribution of mortars with different mix ratios at various curing ages. Based on their impact on the comprehensive properties of mortar, pore sizes are classified into four categories: harmless pores (<20 nm), few-harm pores (20–50 nm), harmful pores (50–200 nm), and multi-harm pores (>200 nm) [34]. MIP tests were conducted on ten groups of mix design specimens at 7 and 28 days, and the total porosity and the porosity of each type of pores are shown in Table 5.

From Table 5, it can be observed that the addition of CSP and RHA reduces the total porosity. This is due to the continuous formation of pozzolanic reaction products that fill the pores, and RHA effectively refines the pore space. It can be observed that R15S10 is more effective in improving pore structure compared to others. At 28 days, the multi-harm pores (>200 nm) decreased from 2.48 % to 1.54 %, which was 53.25 % lower than the control. The total porosity became the smallest at 9.7 %, and the main pore diameter reduced from 26.77 nm to 18.54 nm. Due to the high compressive strength and optimal pore distribution of R15S10 at 28 days, R15

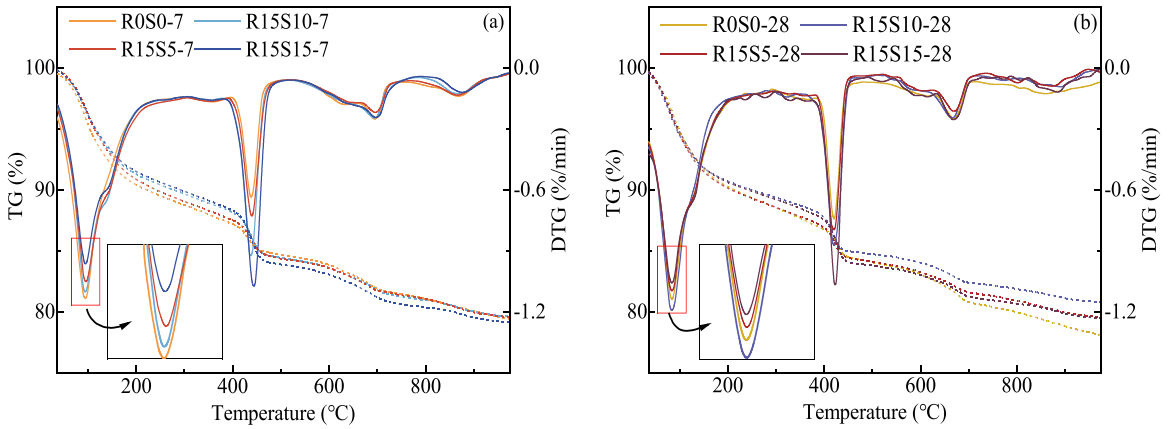

Fig. 11. TG and DTG curves of R0S0, R15S5, R15S10, and R15S15.

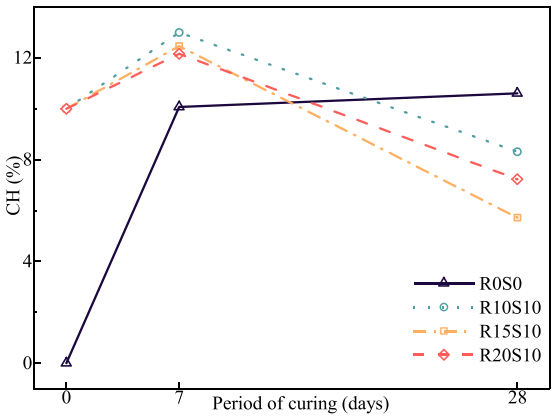

Fig. 12. Free CH (%) of R0S0, R10S10, R15S10 and R20S10.

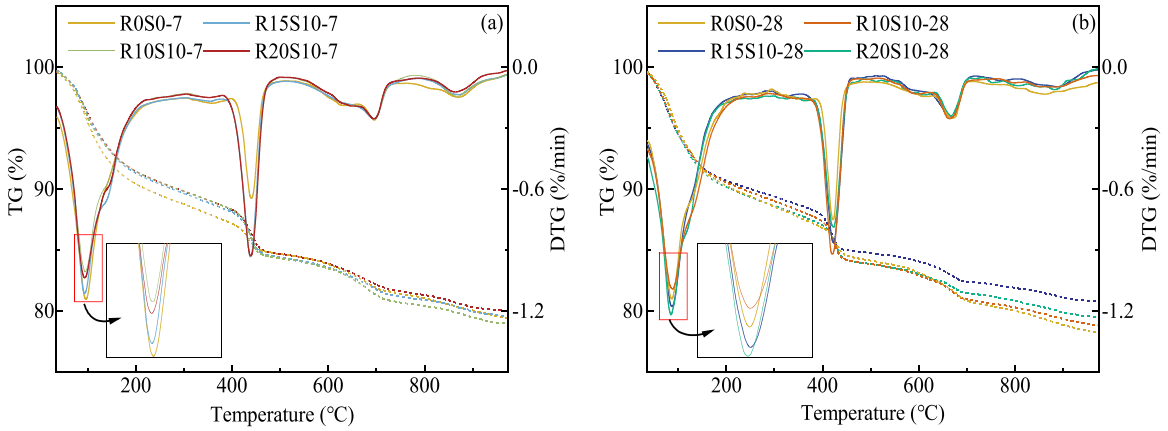

Fig. 13. TG and DTG curves of R0S0, R10S10, R15S10, and R20S10.

Table 4
Thermogravimetric mass loss (%) and free CH (%) of mixtures over different curing ages.

NO.	Mixture design	Ldh(%)	Ldx (%)	Ldc (%)	Ldca (%)	CH (%)
1	R0S0–7d	6.9012	0.9132	5.2924	1.5305	10.0730
2	R0S0–28d	7.9758	0.7533	6.0015	1.5305	10.6076
3	R10S5–7d	7.3404	1.2046	5.2257	1.4329	11.3229
4	R10S5–28d	7.6993	0.8379	5.5871	1.4329	10.4226
5	R10S10–7d	5.5413	1.6580	5.1456	1.4636	13.0003
6	R10S10–28d	6.8310	0.5763	5.0015	1.4636	8.3120
7	R10S15–7d	7.7780	1.8252	5.3415	1.4941	13.9651
8	R10S15–28d	8.4845	0.8698	5.4511	1.4941	10.2227
9	R15S5–7d	6.3108	1.5675	4.7721	1.3689	12.1598
10	R15S5–28d	7.4142	0.5418	4.4898	1.3689	7.4698
11	R15S10–7d	6.7852	1.6460	4.7893	1.3995	12.4600
12	R15S10–28d	9.2972	0.3698	3.9007	1.3995	5.7220
13	R15S15–7d	5.7042	2.0753	4.6928	1.4301	14.0107
14	R15S15–28d	6.8890	0.5377	4.2358	1.4301	6.9236
15	R20S5–7d	7.1070	1.1817	4.6864	1.3048	10.5377
16	R20S5–28d	6.9848	0.5870	4.1488	1.3048	7.1906
17	R20S10–7d	6.1750	1.5999	4.6583	1.3354	12.1579
18	R20S10–28d	9.4502	0.5807	4.2221	1.3354	7.2361
19	R20S15–7d	7.2002	2.1983	4.4779	1.3660	14.2628
20	R20S15–28d	7.8458	0.8096	4.3464	1.3660	8.3343

Table 5
Total porosity and pore distribution of various pore types in the mixtures.

No.	Mixture design	Total porosity (%)	Pore size distribution (%)			
			Harmless pores (20 <nm)	few-harm pores (20–50 nm)	harmful pores (50–200 nm)	multi-harm pores (>200 nm)
1	R0S0–7d	11.6108	2.3045	3.6640	1.9492	3.6931
2	R0S0–28d	10.1918	1.6096	3.1298	2.1628	3.2896
3	R10S5–7d	13.2706	2.7601	4.2490	2.9974	3.2641
4	R10S5–28d	10.0230	2.1903	2.8099	2.4250	2.5978
5	R10S10–7d	12.4337	2.9181	4.2278	2.4718	2.8160
6	R10S10–28d	10.4257	2.3566	3.5493	2.2633	2.2565
7	R10S15–7d	12.8893	4.2970	2.5054	2.7913	3.2956
8	R10S15–28d	10.8316	2.8941	3.5641	1.5357	2.8377
9	R15S5–7d	12.5918	3.3743	3.9505	2.3550	2.9119
10	R15S5–28d	10.4754	2.7746	3.3959	2.1577	2.1472
11	R15S10–7d	11.6937	3.2688	4.0485	1.8943	2.4821
12	R15S10–28d	9.6967	3.1958	2.5203	2.4418	1.5388
13	R15S15–7d	12.2706	2.6881	3.8320	2.5950	3.1555
14	R15S15–28d	10.1806	2.6958	2.5697	2.3017	2.6134
15	R20S5–7d	12.5328	2.5151	4.5185	2.4389	3.0604
16	R20S5–28d	10.5395	3.5340	1.9038	2.6725	2.4293
17	R20S10–7d	12.2648	4.2515	3.2675	2.0341	2.7116
18	R20S10–28d	10.3359	2.8521	2.9887	2.6333	1.8618
19	R20S15–7d	13.4847	2.4717	4.5522	3.0395	3.4214
20	R20S15–28d	11.2967	3.8502	2.0510	2.3371	3.0584

and S10 were used as benchmarks to apply the control variable method to observe the effects of replacement levels on mortar pores. Fig. 14 shows the porosity distribution of the mixtures, comparing the proportion of each value to the total.

Fig. 14(a) and Fig. 15 illustrate the effect of CSP content on mortar porosity. The mixture with 10 % CSP exhibited the lowest total porosity and the fewest multi-harm pores (>200 nm) at both curing ages. In the control group, total porosity decreased minimally from 11.61 % at 7 days to 10.19 % at 28 days due to the absence of pozzolanic reactions. In contrast, CSP-containing mixtures showed greater reductions, attributed to pozzolanic activity enhancing matrix densification and reducing capillary pore volume and connectivity [58]. Increasing CSP content decreased total porosity and refined pore structure, shifting pores towards a harmless size range. R15S15 had the highest total porosity and largest primary pore size but still exhibited lower multi-harm pore values than the control, with reductions of 0.54 % at 7 days and 0.68 % at 28 days. The primary pore size decreased from 35.21 nm to 32.48 nm, representing reductions of 42.35 % and 35.84 %, respectively, compared to the control. Although higher CSP content led to more pores and larger main pore diameters, these values remained lower than the control at the same curing age.

Fig. 14(b) and Fig. 16 illustrate the effect of varying RHA content on mortar performance. The main pore diameters of R10S10, R15S10, and R20S10 decreased to 27.48 nm, 18.54 nm, and 28.28 nm, respectively, with R15S10 showing the most significant reduction. Total porosity decreased by 16.15 %, 17.08 %, and 15.76 %, aligning with compressive strength results, explaining why R15S10 outperformed R10S10 and R20S10. CSP enhances RHA dissolution, increasing amorphous silica and promoting high-density C-S-H gel formation, which refines pores and improves microstructure. This reduces pores > 200 nm, lowering the Ca/Si ratio internally while increasing it externally, altering CH crystallization and weakening its microstructure[8,61]. Increasing RHA from 10 % to 15 % reduced multi-harm pores by 0.94 % and total porosity by 1.99 %, improving compactness. However, raising RHA to

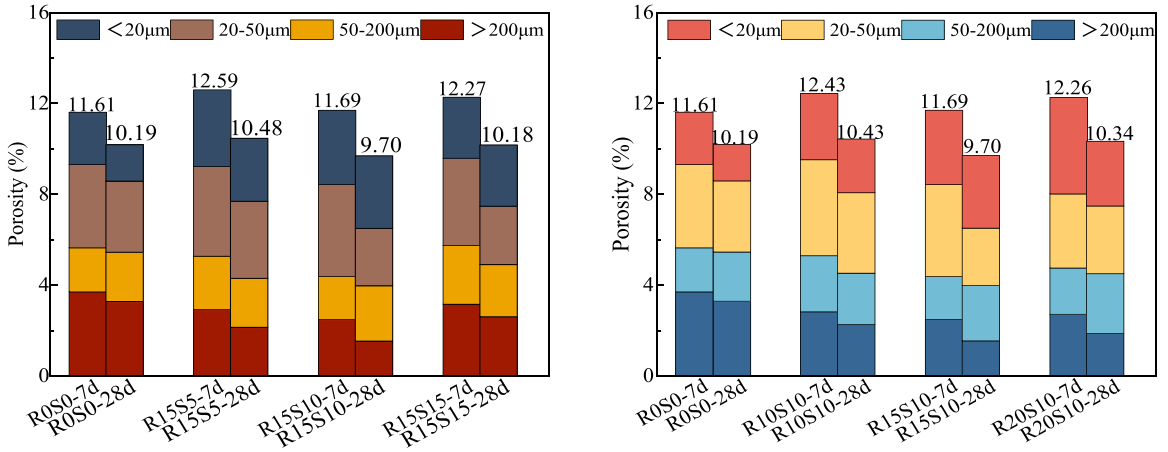

Fig. 14. The porosity distribution of mixtures as a function of curing ages.

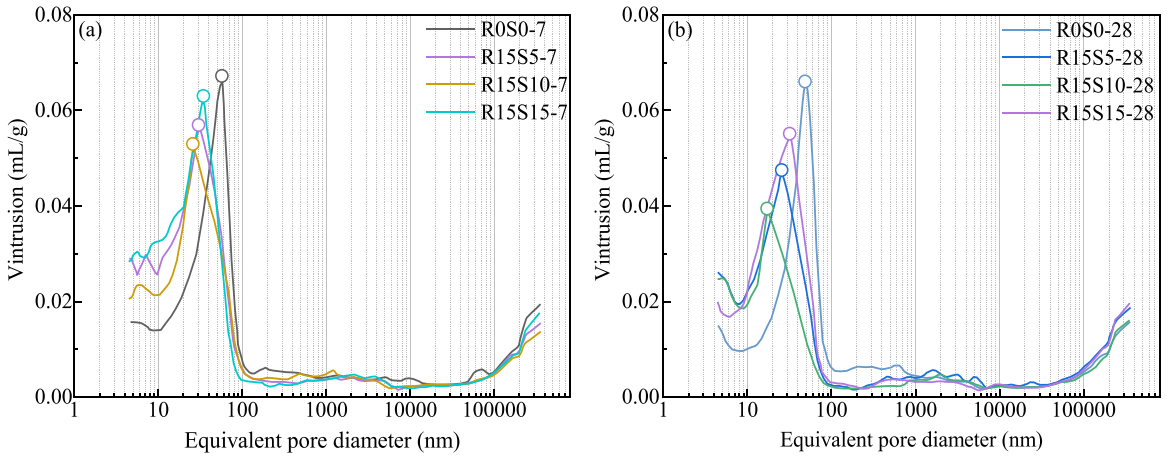

Fig. 15. Pore size distribution curves of R0S0, R15S5, R15S10, and R15S15.

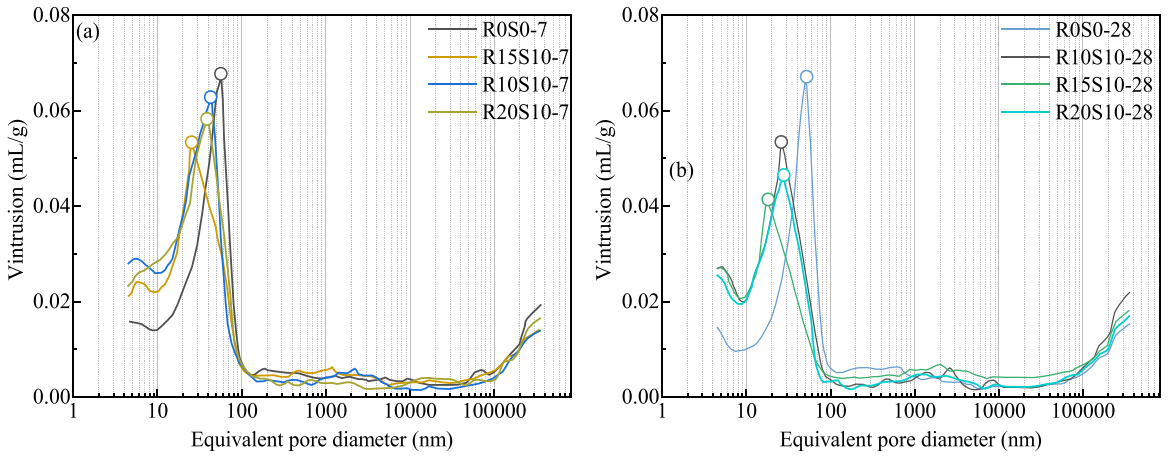

Fig. 16. Pore size distribution curves of R0S0, R10S10, R15S10, and R20S10.

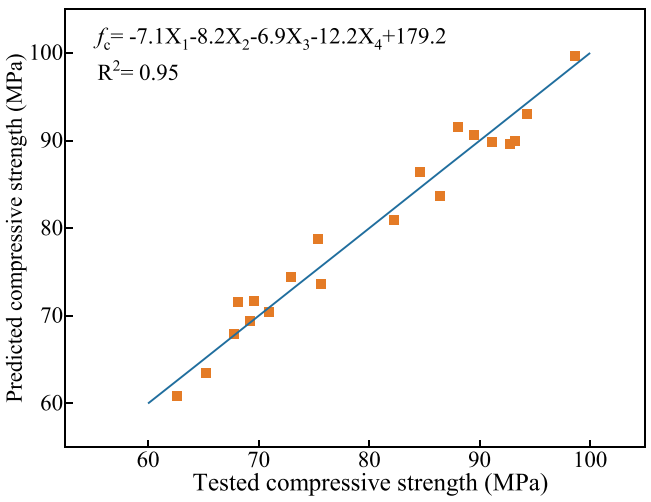

Fig. 17. The relationship between predicted compressive strength and tested compressive strength of mixtures.

20 % resulted in higher porosity (10.34 %) and a larger primary pore size (28.28 nm), reducing refinement efficiency. Excess RHA leads to unreacted silica forming H_4SiO_4, which reacts with Ca^{2+}, increasing silicate chain polymerization. This promotes C-S-H network formation but also enlarges total porosity and primary pore size, diminishing overall structural improvement[25].

According to the macroscopic mechanical properties and TGA results detailed in Sections 3.2 and 3.3, there is a strong correlation between the pore distribution and compressive strength of different mixtures. A quantitative correlation fitting was performed for the compressive strength and pore distribution of ten mixtures, as shown in Fig. 17. The results indicate a good linear relationship between the pore distribution and compressive strength of the mixtures. The coefficient for multi-harm pores (X_4) is −12.2, indicating that a higher quantity of such pores leads to a lower compressive strength of the mortar, consistent with the experimental results.

3.5. Scanning electron microscope

To investigate the changes in the internal microstructure of cement mortar with different RHA and CSP contents, Scanning Electron Microscope (SEM) analyses were conducted at 7 days and 28 days of curing. SEM-BSE images are grayscale, where the grayscale value of each pixel is positively correlated with the atomic number of the element at that point. The higher the atomic number, the greater the grayscale value of the pixel. In the images, areas from bright to dark represent unhydrated cement, hydration products, fine aggregates, and pores. From the SEM images at 7 and 28 days, it can be observed that the cement matrix of the different mixtures becomes denser over time. Since R15S10 has the best mechanical properties and pore distribution at 28 days, we used R15 and S10 as benchmarks and employed the control variable method to observe the impact of different admixture amounts on the microstructure of the mortar. For each mixture ratio in these figures, (a) represents 7 days and (b) represents 28 days.

In Fig. 18, microcracks and pores in R10S10 were primarily observed at the aggregate-cement paste interfacial transition zone at 7 days. This can be attributed to the slow pozzolanic reaction and the small amount of C-S-H gel formation, resulting in lower strength in the interfacial transition zone, coarsening of pores and blurred defect boundaries [36]. The RHA grains have smooth surfaces and remain undissolved, absorbing water during mixing and curing, which reduces the degree of cement hydration at the early stage. Consequently, a large number of unhydrated cement grains with significant volume are observed. At 28 days, the quantity and volume of unhydrated cement grains decreased and RHA gradually dissolved, increasing the solubility of amorphous silica in the matrix [5]. This significantly increases the amount of high-compactness C-S-H gel, which greatly reduces the number of pores and ultimately lowering the Ca/Si ratio and enhancing the microstructure of internal hydration products.

Fig. 19 illustrates that in R15S5, RHA initially acts as a filler, partially occupying pores at 7 days. However, its increased content raises mortar viscosity, trapping air voids within the matrix and around RHA particles. As curing progresses, RHA reacts with CH in a pozzolanic reaction, forming C-S-H gel, which, along with unreacted or partially reacted RHA, fills these voids. This process refines the pore structure and enhances compressive strength in later stages. However, some fine RHA particles remain unreacted, likely due to insufficient CH availability [36,55].

Fig. 20 shows that in R15S10, RHA undergoes pozzolanic reactions with CH, forming needle-like C-S-H on its surface by 7 days. However, larger RHA particles remain intact. By 28 days, finer RHA particles dissolve, producing substantial C-S-H gel that fills pores, while larger RHA grains begin reacting, forming filamentous hydration products. The interfacial transition zone between the cement matrix and aggregate becomes more compact and seamless. RHA promotes CH consumption, further accelerating pozzolanic activity by reducing calcium ion concentration and dissolving calcium-rich phases [29,36]. The cement matrix exhibits increased density over time, with fewer unhydrated cement particles, aligning with reduced porosity and improved compressive strength.

Fig. 21 illustrates the R15S15 mortar at 7 days features numerous large-diameter, elongated, and interconnected deep pores, with a considerable amount of unhydrated cement grains remaining. Due to the 15 % CSP content, a large amount of CH is present in the matrix, which weakens the strength of the interfacial transition zone. At 7 days, the resulting C-S-H was relatively loose and flocculent, not fully occupying the entire pores, which corresponded to the low early strength and high porosity [29]. At 28 days, RHA gradually dissolved and formed honeycomb-like hydration products to fill the pores. The amount of C-S-H increases, enhancing the matrix compactness, although residual CH can still be observed.

At 7 days, R20S10 exhibits an uneven microstructure with many unreacted or partially reacted RHA. Some RHA spherical grains are

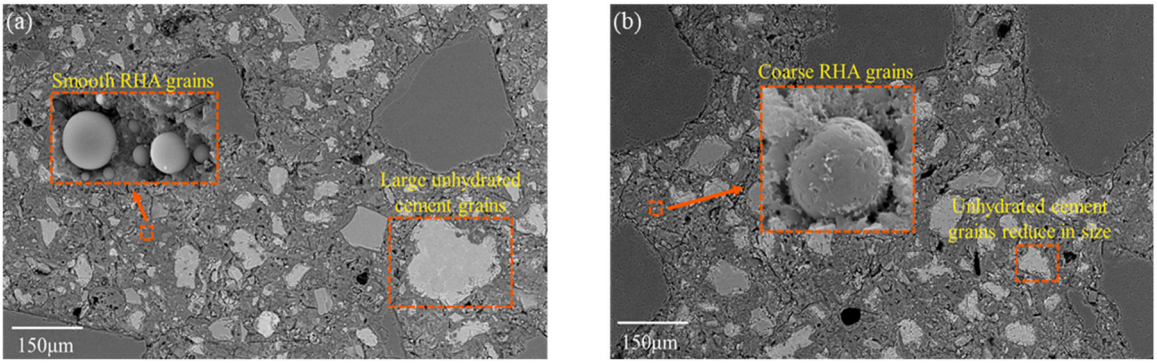

Fig. 18. SEM-BSE images of R10S10.

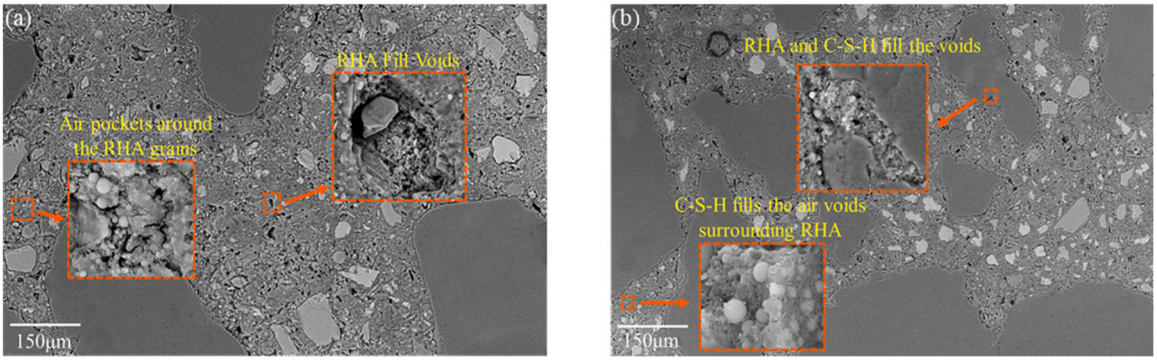

Fig. 19. SEM-BSE images of R15S5.

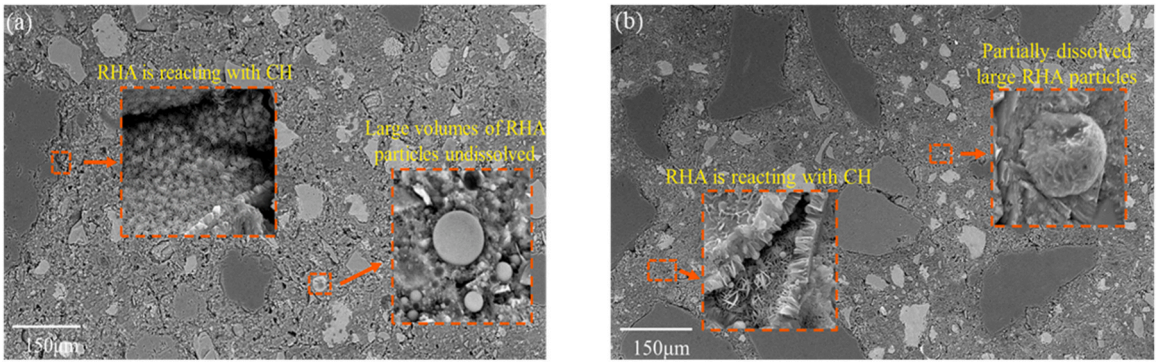

Fig. 20. SEM-BSE images of R15S10.

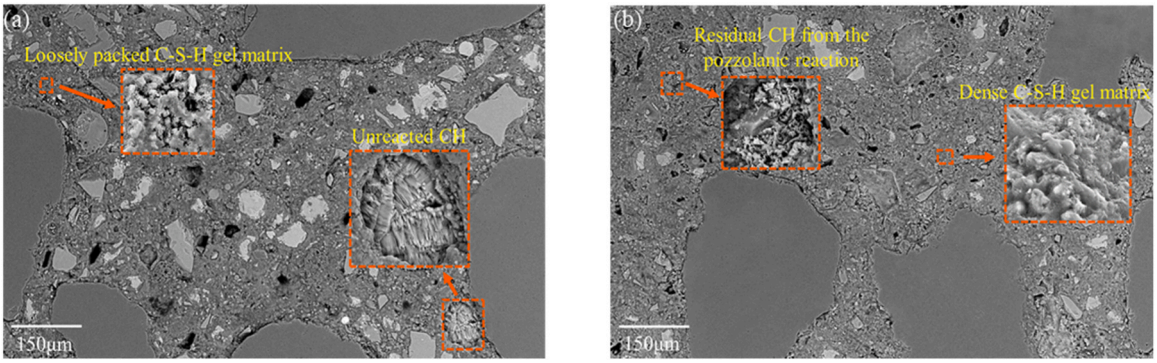

Fig. 21. SEM-BSE images of R15S15.

firmly embedded in the microstructure, indicating that the strength of the unreacted or partially reacted RHA and their bonding with the matrix may significantly affect the overall strength of the concrete [30]. As the curing ages increase, the images exhibit a denser microstructure, corresponding to its improved mechanical properties. Due to ongoing hydration and pozzolanic reactions, C-A-S-H and C-S-H gels coexist, increasing the packing compactness within the microstructure [27]. C-S-H fills the voids in the interfacial transition zone between the cement and RHA, thereby enhancing its strength (Fig. 22).

3.6. Sustainability indicator calculation

The total carbon emissions, embodied energy, and production costs for four specimen groups—R0S0, R15S5, R15S10, and R15S15—were evaluated. Baseline values for raw material carbon emissions, embodied energy, and production costs were referenced from [62,63]. Using R0S0 as the benchmark, the percentage change in these indicators was calculated for each specimen over its life cycle. This analysis determined the carbon emissions, embodied energy, and production costs associated with producing 1 m^3 of

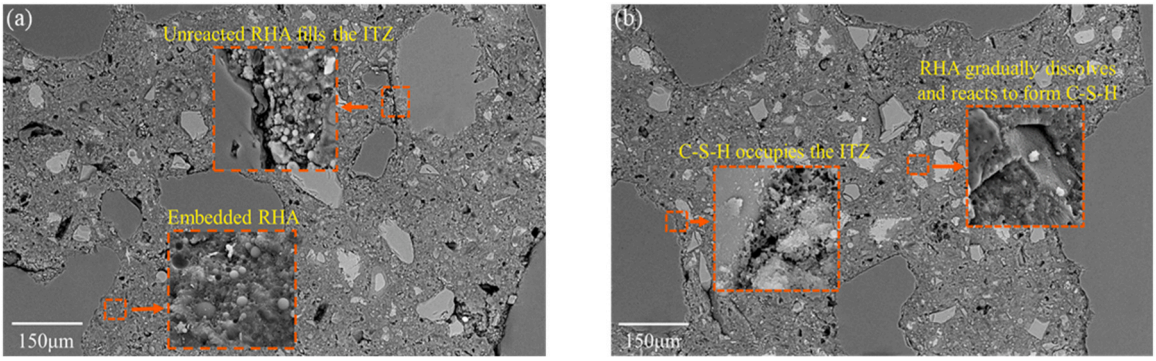

Fig. 22. SEM-BSE images of R20S10.

cement mortar at varying CSP replacement levels. The results are presented in Fig. 23.

As illustrated in Fig. 23, increasing the CSP content reduces the carbon emissions, embodied energy, and production costs associated with producing 1 m^3 of cement mortar. Regarding carbon emissions, although CSP releases CO_2 during production, its emissions are significantly lower than those of cement. Thus, replacing cement with CSP effectively reduces the overall carbon footprint of cement mortar. With a constant RHA dosage, increasing the CSP content from 5 % to 15 % lowers carbon emissions from 679.7 kg to 652.7 kg, equating to a reduction of approximately 1.7 kg of CO_2 per 1 % cement replacement by CSP. Similarly, embodied energy analysis reveals that CSP production consumes significantly less energy than cement. As a result, incorporating CSP into the mix substantially decreases the energy demand of mortar production. When CSP and RHA are both used at 15 %, the embodied energy required to produce 1 m^3 of mortar decreases by 20 %. Although CSP reduces cement mortar production costs, the impact is modest due to the high price of silica sand. A cost comparison indicates that the production cost of 1 m^3 of R0S0 cement mortar (cement only) is 372.5 yuan, whereas for 1 m^3 of R15S15 cement mortar (cement + RHA + CSP), the cost is 337.7 yuan—a 9.34 % reduction. These findings highlight the economic and environmental benefits of utilizing biomass waste in cement mortar production.

4. Conclusions

This study explored the integration of two sustainable materials, rice husk ash (RHA) and calcined shell powder (CSP), to assess their effects on strength development, phase composition, and microstructural evolution in cement mortar. Among the tested mixtures, R15S10 demonstrated the most balanced performance. The key findings are as follows.

(1) Partial cement replacement with RHA and CSP significantly enhanced compressive strength, particularly at later curing stages. R15S10 exhibited the highest mechanical performance at 28 days.

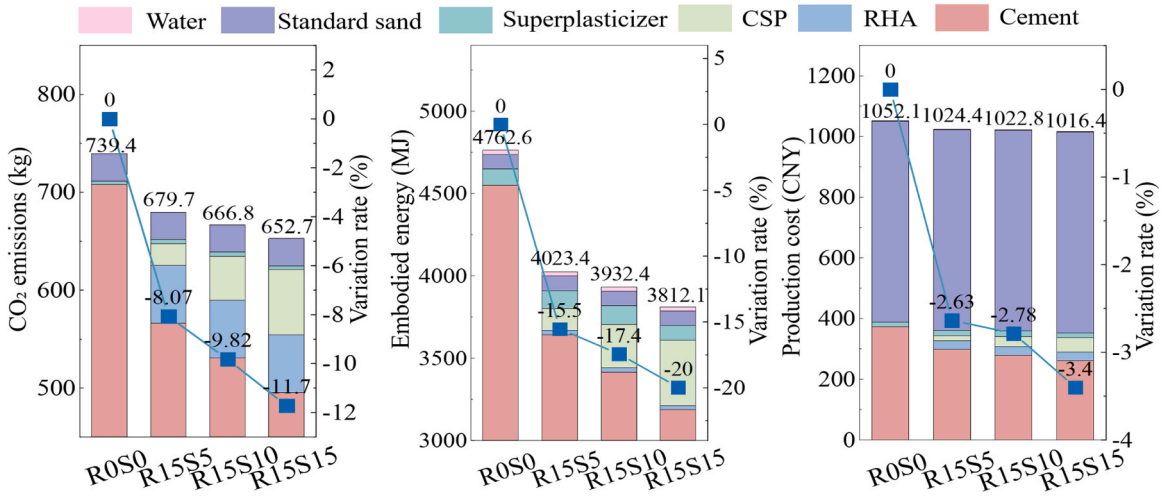

(a) CO_2 emissions *(b) Embodied energy* *(c) Production cost (CNY)*

Fig. 23. Carbon emissions, embodied energy, and production cost of different specimens.

(2) The high reactivity and porosity of RHA and CSP increased water demand, requiring additional superplasticizer to maintain target workability (240 mm ± 5 %).
(3) TGA revealed that residual CH content varied with different RHA and CSP proportions and curing ages, directly affecting the extent of the pozzolanic reaction. R15S10 exhibited the highest C-S-H dehydration peak and the lowest residual CH, contributing to its superior performance.
(4) The addition of CSP and RHA reduced overall porosity and refined the pore structure. R15S10 achieved the greatest improvement, with a notable reduction in multi-harm pores and primary pore diameter, enhancing mortar compactness.
(5) Microcracks and pores primarily formed in the interfacial transition zone between the aggregate and cement paste, particularly in early curing stages.

CRediT authorship contribution statement

Ye Li: Visualization, Supervision, Methodology, Conceptualization; **Hangqi Lou:** Supervision, Software, Methodology, Investigation, Data curation; **Shiyu Zhuang:** Writing – review & editing, Resources, Project administration, Investigation, Conceptualization; **Yutao Guo:** Writing – review & editing, Validation, Supervision, Resources, Project administration, Methodology, Funding acquisition, Conceptualization; **Jiaxi Zhang:** Writing – original draft, Visualization, Validation, Software, Resources, Project administration, Methodology, Investigation, Formal analysis, Data curation, Conceptualization

Declaration of Competing Interest

The authors declare that they have no known competing financial interests or personal relationships that could have appeared to influence the work reported in this paper.

Acknowledgements

The authors gratefully acknowledge the financial support provided by the National Natural Science Foundation of China, Grant No. 52308179 and by the Shenzhen Municipal Finance Bureau, Grant No. QD2022023C. The authors would also like to thank Tsinghua Shenzhen International Graduate School, Harbin Institute of Technology (Shenzhen), and China Building Technology Center for providing the facilities and experimental instruments.

Data Availability

Data will be made available on request.

References

[1] Y. Han, Z. Yang, T. Ding, J. Xiao, Environmental and economic assessment on 3D printed buildings with recycled concrete, J. Clean. Prod. 278 (2021) 123884.
[2] X. Cao, X. Li, Y. Zhu, Z. Zhang, A comparative study of environmental performance between prefabricated and traditional residential buildings in China, J. Clean. Prod. 109 (2015) 131–143.
[3] A.N. Givi, S.A. Rashid, F.N. Aziz, M.A. Salleh, Assessment of the effects of rice husk ash particle size on strength, water permeability and workability of binary blended concrete, Constr. Build. Mater. 24 (2010) 2145–2150.
[4] M. Nehdi, J. Duquette, A. El Damatty, Performance of rice husk ash produced using a new technology as a mineral admixture in concrete, Cem. Concr. Res. 33 (2003) 1203–1210.
[5] A.A. Boateng, D.A. Skeete, Incineration of rice hull for use as a cementitious material: the Guyana experience, Cem. Concr. Res. 20 (1990) 795–802.
[6] M.A. Jamil, et al., Curing effects on geotechnical properties of clays treated with palm kernel shell ash and rice husk ash: Insights from water absorption characteristics of stabilizers, Case Stud. Constr. Mater. 20 (2024) e02947.
[7] M.A. Jamil, et al., Consolidation characteristics of compacted clayey soils treated with various biomass ashes, Results Eng. 24 (2024) 103480.
[8] D.G. Nair, A. Fraaij, A.A.K. Klaassen, A.P.M. Kentgens, A structural investigation relating to the pozzolanic activity of rice husk ashes, Cem. Concr. Res. 38 (2008) 861–869.
[9] A.Y. Elghazouli, A. Mujdeci, D.V. Bompa, et al., Experimental cyclic response of rubberised concrete-filled steel tubes, J. Constr. Steel Res. 199 (2022) 107622.
[10] A.Y. Elghazouli, A. Mujdeci, D.V. Bompa, Y. Guo, Experimental cyclic response of rubberised concrete-filled steel tubes, J. Constr. Steel Res. 199 (2022) 107622.
[11] M. Sandanayake, Y. Bouras, R. Haigh, Z. Vrcelj, Current sustainable trends of using waste materials in concrete—a decade review, Sustainability 12 (2020) 9622.
[12] B.N. Al-Kharabsheh, et al., Basalt fiber reinforced concrete: a compressive review on durability aspects, Mater 16 (2023) 429.
[13] K.C. Onyelowe, et al., Global warming potential-based life cycle assessment and optimization of the compressive strength of fly ash-silica fume concrete; environmental impact consideration, Front. Built Environ. 8 (2022) 992552.
[14] Y. Guo, X. Nie, M. Tao, et al., Selected series method on buckling design of stiffened steel-concrete composite plates, J. Constr. Steel Res. 161 (2019) 296–308.
[15] Y. Guo, M. Alam, Nonlinear bending and thermal postbuckling of magneto-electro-elastic nonlocal strain-gradient beam including surface effects, Appl. Math. Model. (2025) 115955.
[16] M. Alam, Y. Guo, Y. Bai, S.H. Luo, Post-critical nonlinear vibration of nonlocal strain gradient beam involving surface energy effects, J. Sound Vib. (2025) 118930.
[17] A. Geethakarthi, Novel approaches towards sustainable management of an agricultural residue—the rice husk, Nat. Environ. Pollut. Technol. 20 (1) (2021).
[18] H.Y. Wang, D.L. Wang, J.Z. Li, et al., Estimation and utilization of rice husk resources in China, Jiangsu Agric. Sci. 40 (2012) 298–300.
[19] J.P. Morris, T. Backeljau, G. Chapelle, Shells from aquaculture: a valuable biomaterial, not a nuisance waste product, Rev. Aquac. 11 (2019) 42–57.
[20] C. Martínez-García, B. González-Fonteboa, F. Martínez-Abella, D. Carro-López, Performance of mussel shell as aggregate in plain concrete, Constr. Build. Mater. 139 (2017) 570–583.
[21] G.O. Bamigboye, A.T. Nworgu, A.O. Odetoyan, M.A. Kareem, D.O. Enabulele, D.E. Bassey, Sustainable use of seashells as binder in concrete production: prospect and challenges, J. Build. Eng. 34 (2021) 101595.

[22] K.C. Onyelowe, A.M. Ebid, M.R. Ghadikolaee, GRG-optimized response surface powered prediction of concrete mix design chart for the optimization of concrete compressive strength based on industrial waste precursor effect, Asian J. Civ. Eng. 25 (2024) 997–1006.
[23] C. Garcia, et al., Predicting the impact of adding metakaolin on the splitting strength of concrete using ensemble ML classification and symbolic regression techniques–a comparative study, Front. Built Environ. 10 (2024) 1395448.
[24] K.C. Onyelowe, et al., Estimating the compressive strength of lightweight foamed concrete using different machine learning-based symbolic regression techniques, Front. Built Environ. 10 (2024) 1446597.
[25] K. Ganesan, K. Rajagopal, K. Thangavel, Rice husk ash blended cement: assessment of optimal level of replacement for strength and permeability properties of concrete, Constr. Build. Mater. 22 (2008) 1675–1683.
[26] A. Siddika, M.A. Mamun, R. Alyousef, H. Mohammadhosseini, State-of-the-art-review on rice husk ash: a supplementary cementitious material in concrete, J. King Saud. Univ. - Eng. Sci. 33 (2020) 294–307.
[27] M.C.G. Juenger, R. Siddique, Recent advances in understanding the role of supplementary cementitious materials in concrete, Cem. Concr. Res. 73 (2015) 71–80.
[28] M. Jamil, A.B.M.A. Kaish, S.N. Raman, M.F.M. Zain, Pozzolanic contribution of rice husk ash in cementitious system, Constr. Build. Mater. 47 (2013) 588–593.
[29] R.S. Bie, X.F. Song, Q.Q. Liu, X.Y. Ji, P. Chen, Studies on effects of burning conditions and rice husk ash (RHA) blending amount on the mechanical behavior of cement, Cem. Concr. Compos. 55 (2015) 162–168.
[30] S.H. Kang, S.G. Hong, J. Moon, The use of rice husk ash as reactive filler in ultra-high performance concrete, Cem. Concr. Res. 115 (2019) 389–400.
[31] Y. Liao, J. Fan, R. Li, B. Da, D. Chen, Y. Zhang, Influence of the usage of waste oyster shell powder on mechanical properties and durability of mortar, Adv. Powder Technol. 33 (2022) 103503.
[32] U.G. Eziefula, J.C. Ezeh, B.I. Eziefula, Properties of seashell aggregate concrete: a review, Constr. Build. Mater. 192 (2018) 287–300.
[33] H. Wang, R.J.O. Connell, D. Lee, Experimental analysis on calcination and carbonation process in calcium looping for CO2 capture: study case of cement plants in Indonesia (published online), Clean. Energy (2023).
[34] J.A. González, J.L. Rivera, A.G. González, S.M. Martínez, R.A. Berenguer, Properties of cementitious materials utilizing seashells as aggregate or cement: prospects and challenges, Materials 13 (2020) 4321.
[35] W. Zhao, X. Ji, Y. Jiang, T. Pan, Effect of C-S-H nucleating agent on cement hydration, Appl. Sci. 11 (2021) 6638.
[36] P.A. Adesina, F.A. Olutoge, Structural properties of sustainable concrete developed using rice husk ash and hydrated lime, J. Build. Eng. 25 (2019) 100804.
[37] A. Cuesta, I. Santacruz, G. Angeles, M. Dapiaggi, J.D. Zea-Garcia, M.A. Aranda, Local structure and Ca/Si ratio in CSH gels from hydration of blends of tricalcium silicate and silica fume, Cem. Concr. Res. 143 (2021) 106405.
[38] P. Ghoddousi, L. Adelzade Saadabadi, Study on hydration products by electrical resistivity for self-compacting concrete with silica fume and metakaolin, Constr. Build. Mater. 154 (2017) 219–228.
[39] P. Chindaprasirt, C. Jaturapitakkul, T. Sinsiri, Effect of fly ash fineness on microstructure of blended cement paste, Constr. Build. Mater. 21 (2007) 1534–1541.
[40] J. Payá, J. Monzó, M.V. Borrachero, E. Peris-Mora, F. Amahjour, Mechanical treatment of fly ashes: Part IV. Strength development of ground fly ash-cement mortars cured at different temperatures, Cem. Concr. Res. 30 (2000) 543–551.
[41] Y.M. Zhang, W. Sun, H.D. Yan, Hydration of high-volume fly ash cement pastes, Cem. Concr. Compos. 22 (2000) 445–452.
[42] L.H.P. Silva, V. Nehring, F.F.G. de Paiva, et al., Synergistic effects of limestone powder and unground rice husk ash additions on performances of slag-cement based self-compacting concrete, Mater. Struct. 56 (2023) 65.
[43] H. Lu, Q. Sun, Preparation and strength formation mechanism of calcined oyster shell, red mud, slag, and iron tailing composite cemented paste backfill, Materials 15 (2022) 2199.
[44] A. ElNemr, Generating water/binder ratio-to-strength curves for cement mortar used in masonry walls, Constr. Build. Mater. 233 (2020) 117249.
[45] Z.H. He, et al., Recycling of water treatment sludge in concrete: the role of water-binder ratio from a nanoscale perspective, Sci. Total Environ. 873 (2023) 162456.
[46] Y. Li, et al., Effect of post-fire lime-saturated water and water–CO2 cyclic curing on strength recovery of thermally damaged high-performance concrete with different silica contents, Cem. Concr. Res. 164 (2023) 107050.
[47] T.J. Liu, et al., Strength recovery of thermally damaged high-performance concrete subjected to post-fire carbonation curing, Cem. Concr. Compos. 143 (2023) 105273.
[48] National Cement Standardization Technical Committee, GB/T 17671-2021, Test method of cement mortar strength (ISO method), Stand. Adm. People's Repub. China Beijing (2021).
[49] R. Snellings, A. Bazzoni, K. Scrivener, The existence of amorphous phase in Portland cements: Physical factors affecting Rietveld quantitative phase analysis, Cem. Concr. Res. 59 (2014) 139–150.
[50] Y.J.N. Djobo, A. Elimbi, J. Dika Manga, I.B. Djon Li Ndjock, Partial replacement of volcanic ash by bauxite and calcined oyster shell in the synthesis of volcanic ash-based geopolymers, Constr. Build. Mater. 113 (2016) 673–681.
[51] D. Ciancio, C.T.S. Beckett, J.A.H. Carraro, Optimum lime content identification for lime-stabilised rammed earth, Constr. Build. Mater. 53 (2014) 59–65.
[52] M. Singh, R. Siddique, Strength properties and micro-structural properties of concrete containing coal bottom ash as partial replacement of fine aggregate, Constr. Build. Mater. 50 (2014) 246–256.
[53] E. Mohseni, F. Naseri, R. Amjadi, M.M. Khotbehsara, M.M. Ranjbar, Microstructure and durability properties of cement mortars containing nano-TiO2 and rice husk ash, Constr. Build. Mater. 114 (2016) 656–664.
[54] P.K. Mehta, Properties of blended cements made from rice husk ash, J. Am. Concr. Inst. 74 (1977) 440–442.
[55] G.C. Cordeiro, R.D. Toledo Filho, L.M. Tavares, E.M.R. Fairbairn, Ultrafine grinding of sugar cane bagasse ash for application as pozzolanic admixture in concrete, Cem. Concr. Res. 39 (2009) 110–115.
[56] V. Saraswathy, S. Ha-Won, Corrosion performance of rice husk ash blended concrete, Constr. Build. Mater. 21 (2007) 1779–1784.
[57] S.N. Raman, T. Ngo, P. Mendis, H.B. Mahmud, High-strength rice husk ash concrete incorporating quarry dust as a partial substitute for sand, Constr. Build. Mater. 25 (2011) 3123–3130.
[58] A. Joshaghani, M.A. Moeini, Evaluating the effects of sugar cane bagasse ash (SCBA) and nanosilica on the mechanical and durability properties of mortar, Constr. Build. Mater. 152 (2017) 818–831.
[59] I. Pane, W. Hansen, Investigation of blended cement hydration by isothermal calorimetry and thermal analysis, Cem. Concr. Res. 35 (2005) 1155–1164.
[60] S.K. Agarwal, Pozzolanic activity of various siliceous materials, Cem. Concr. Res. 36 (2006) 1735–1739.
[61] J. Wang, J. Xie, L. Tang, J. Song, Rheological properties, compressive strength, hydration products and microstructure of seawater-mixed cement pastes, Cem. Concr. Compos. 114 (2020) 103770.
[62] S.S. Xing, E. Dong, J.S. Liu, et al., Environmental impact assessment of rice husk ash cement mortar, J. Wuhan. Univ. Technol. 36 (2017) 61–66 (In Chinese).
[63] V. Ediger, S. Akar, ARIMA forecasting of primary energy demand by fuel in Turkey, Energy Policy 35 (2007) 1701–1708.